Composites: Part A 163 (2022) 107237

Contents lists available at ScienceDirect

Composites Part A

journal homepage: www.elsevier.com/locate/compositesa

Shape memory polyimides and composites with tunable chain stiffness and ultrahigh transition temperature range

Xiaofei Wang, Yang He *, Jinsong Leng *

Center for Composite Materials and Structures, Harbin Institute of Technology, Harbin 150080, PR China

ARTICLE INFO

Keywords:
A. Polymer-matrix composites
A. Smart Material
B. High-temperature Properties
E. Heat treatment

ABSTRACT

Shape memory polymer has shape morphing capabilities upon external stimuli, including thermal-, electro-, magnetic-, photo-, and so on. Among them, shape memory polyimide (SMPI) has excellent thermal stability, creep resistance, radiation resistance, and good mechanical properties, which can be applied in various fields. In this paper, 5-amino-2-(4-aminophenyl) benzimidazole, 2-(4-aminophenyl) benzoxazol-5-amine, and 3,3′,4,4′-biphenyltetracarboxylic dianhydride are utilized to synthesize two semi-trapezoidal aromatic heterocyclic SMPIs with tunable chain stiffness, including imidazole-based shape memory polyimide (M-SMPI) and oxazole-based shape memory polyimide (E-SMPI). Because of asymmetric imidazole groups, M-SMPI has the highest SMPI transition temperature in the world, at 416 ℃. Additionally, the M-SMPI/CF composite also has the highest SMPIC (shape memory polyimide composite) transition temperature, at 399 ℃. Thus, M-SMPI and M-SMPI/CF composites can be used as smart materials in deformable flexible electrodes, high temperature aerospace devices and deployable structures.

1. Introduction

Shape memory polymer composite (SMPC) is a kind of smart material that holds "programmed" temporary shape and recovers the original shape due to the action of thermal field, light irradiation, electric field, magnetic field, chemical solvent or other external stimuli [1–8]. For the thermal responsive SMPC, the sample is heated to the transition temperature T_{trans} (T_{trans} is the shape memory transition temperature, which is glass transition temperature or melting transition temperature). After that, the temporary shape of the thermal responsive SMPC is programmed by external force, and is fixed when the temperature is lower than the T_{trans}. At last, the thermal responsive SMPC can recover the original shape when heats over the T_{trans} [9–12]. In 1940, Mather was the first one to propose "elastic memory" [13], and shape memory materials had begun to attract researchers' intensive attention. Nowadays, SMPC has become another hot research area after shape memory alloy (SMA) [14,15]. Compared with SMA, SMPC has the advantages of light weight, low cost, easy processing, large deformation, and can respond to a variety of stimuli [16–20].

Polyimide has great high and low temperature resistance, low coefficient of thermal expansion, high mechanical properties, high electrical insulation, radiation resistance, excellent flame retardance and self-extinguishment, etc., and, it also has the features of space materials such as low volatility in vacuum [21,22], and can be processed into polyimide films [23], engineering plastics with high temperature resistant [24], resin matrix for composites [25], high temperature resistant binders [26], fibers [27] and etc., so it has tremendous commercial value and promising development in aerospace, microelectronics, precision machinery, and medical devices fields [28–30]. The shape memory polyimide (SMPI) and its composites are expected to be used in sensors, deployable structures and other areas due to its excellent shape memory effect, thermal stability, radiation resistance, and good mechanical properties [31–36].

Researchers have made many reports on SMPI with high shape memory transition temperature. For example, the cage polysilsesquioxane was grafted into the SMPI molecular structure to prepare a light color transparent organic–inorganic hybrid SMPI with glass transition temperature (T_g) or T_{trans} of 351 ℃–372 ℃ [37]. Yu et al. produced series of SMPIs by copolymerization of 4,4′- diaminodiphenyl ether (ODA), 5,4′-diamino-2-phenylbenzimidazole (DAPBI) and benzophenone-3,3′,4,4′-tetracarboxylic dianhydride (BTDA) [38]. By adjusting the ratio of rigid DAPBI to flexible ODA monomers, the thermomechanical properties of the SMPIs changed accordingly. And the synthesized PI-80 has good comprehensive properties, and the glass

* Corresponding authors.
E-mail addresses: yang.he@hit.edu.cn (Y. He), lengjs@hit.edu.cn (J. Leng).

https://doi.org/10.1016/j.compositesa.2022.107237
Received 18 July 2022; Received in revised form 27 September 2022; Accepted 30 September 2022
Available online 7 October 2022
1359-835X/

transition temperature rose from 280 ℃ to 370 ℃. Xiao et al. prepared the SMPI films based on benzoxazole diamine and 4,4′-(hexafluoroisopropylidene) diphthalic anhydrid, of which the T_g was 363 ℃ [39]. Wang et al. prepared poly(benzoxazole-*co*-imide)s by BPDA with two different diamine of 4,4′-oxydianiline (ODA) and 5-amino-2-(4-aminobenzene) benzoxazole, of which the shape memory transition temperature range was 240-350℃, and shape fixity was above 98% and shape recovery was up to 98%. Besides, the multiple-shape memory effects with high switching temperatures were first achieved in poly (benzoxazole-*co*-imide)s [40]. Besides, the authors prepared two kinds of high temperature shape memory copolyimides, and the glass transition temperature of poly(benzoxazole-*co*-imide) (PI1) and poly(benzimidazole-*co*-imide) (PI2) were 280 ℃ and 355 ℃, respectively. Interestingly, shape memory cycles induced orientation with ordered macromolecular chains packing was formed for PI2 after several thermal mechanical cycles, and, the shape recovery ratio was risen from 60% to over 90% after five cycles [41]. At present, the shape memory transition temperature of SMPI is mostly in the range of 200 °C–370 °C. These SMPIs are the SMPs with high transition temperatures, but there is almost no report on the transition temperature that exceeds 380 °C, or reaches 400 °C. Therefore, in this paper, we define that the SMPI with transition temperatures over 380 °C had an ultrahigh transition temperature range.

For the SMPI with high shape transition temperature, the rigid molecular structures such as imidazole ring, oxazole ring, thiazole ring, and benzene ring can improve the thermal stability and rigidity of the polymer [42]. Therefore, in this paper, 5-amino-2-(4-aminophenyl) benzimidazole, 2-(4-aminophenyl) benzoxazol-5-amine, 3,3′,4,4′-biphenyltetracarboxylic dianhydride are used to prepare semi trapezoidal aromatic heterocyclic polyimides, in order to construct SMPI films with the T_{trans} higher than 380 ℃. The innovations are as follows: two kinds of semi trapezoidal aromatic heterocyclic SMPIs including imidazole-based SMPI and oxazole-based SMPI are prepared. The T_{trans} of the imidazole-based SMPI (M-SMPI) is more than 400 ℃, which is the highest shape memory transition temperature of the SMPI film in the world, so the SMPI film with tunable chain stiffness can expand the application range of the smart polymer. On the other side, M-SMPI and carbon fiber twill fabrics are compounded together to prepare shape memory composite M-SMPI/CF, which can be used as skin materials for the morphing aerospace devices and deployable structures, etc.

2. Experimental section

2.1. Materials

3,3′,4,4′-biphenyltetracarboxylic dianhydride (BPDA), 5-amino-2-(4-aminophenyl) benzimidazole (DAPBI), 2-(4-aminophenyl)benzoxazol-5-amine (AAB), and dimethyl sulfoxide (DMSO) all came from Shanghai Aladdin Reagent Co., LTD. The carbon-fiber twill fabric (T300-3 K, the diameter of the fiber is 1 um, and the linear density is 1 dtex, and the rupture specific strength is 1 cN/dtex, and the temperature resistance is 2000 ℃.) was from Japan Toray Co., LTD. N, *N*-dimethylacetamide (DMAc) came from Tianjin Fengchuan Chemical Reagent Technology Co., LTD.

2.2. Preparation of imidazole-based shape memory polyimide (M-SMPI)

(I) At room temperature, 1 mol DAPBI was added to the DMSO solvent, then, 1 mol BPDA was also added to the solution 4–6 times in N_2 atmosphere, and the stirring speed was 250 r/min, and had reacted for 120 h to prepare a polyamic acid (PAA) solution.

(II) The PAA solution was poured on a glass balance plate and had a thermal imidization process, which synthesized the semi trapezoidal aromatic heterocyclic shape memory polyimide film (M-SMPI). The heating steps were as follows: 50 ℃ for 5 h, 80 ℃ for 5 h, 120 ℃ for 2 h, 160 ℃ for 2 h, 200 ℃ for 2 h, 250 ℃ for 2 h, and 300 ℃ for 2 h. The reaction route was shown in Fig. 1a.

2.3. Preparation of oxazole-based shape memory polyimide (E-SMPI)

(I) At room temperature, 1 mol AAB was added to the DMAc solvent, then, 1 mol BPDA was added to the solution 4–6 times in N_2 atmosphere, and the stirring speed was 250 r/min, and had reacted for 120 h to prepare a polyamic acid (PAA) solution.

(II) The PAA solution was poured on a glass balance plate and had a thermal imidization process, which synthesized the semi trapezoidal aromatic heterocyclic shape memory polyimide film (E-SMPI). The heating steps were as follows: 50 ℃ for 5 h, 80 ℃ for 5 h, 120 ℃ for 2 h, 160 ℃ for 2 h, 200 ℃ for 2 h, 250 ℃ for 2 h, and 300 ℃ for 2 h. The reaction route was shown in Fig. 1b.

2.4. Preparation of imidazole-based shape memory polyimide/carbon fiber twill fabric composite (M-SMPI/CF)

(I) At room temperature, 1 mol DAPBI was added to the DMSO solvent, then, 1 mol BPDA was also added to the solution 4–6 times in N_2 atmosphere, and the stirring speed was 250 r/min, and had reacted for 120 h to prepare a polyamic acid (PAA) solution.

(II) The carbon fiber twill fabric was dipped into the polyamic acid solution of step (I), and the solvent was evaporated in a vacuum environment at 50 °C until it was removed completely. The mass ratio of the fiber to the resin matrix was 1:1.

(III) The polyamic acid/carbon fiber twill fabric composite was pre-pressed by a hot press, and the pre-pressing conditions were 3–5 MPa for 180 °C, 10 min; 250 °C, 60 min.

(IV) The pre-pressed SMPI composites were cured secondary, and the curing conditions were as follows: heating to 250 °C for 2 h; 300 °C for 3 h, named M-SMPI/CF. The M-SMPI/CF included 1–4 layers of carbon fiber twill fabric composites, named M-SMPI/1CF, M-SMPI/2CF, M-SMPI/3CF and M-SMPI/4CF, respectively. The preparation route was shown in Fig. 1c.

2.5. Characterization

The chemical group of M-SMPI and E-SMPI were tested by FTIR spectrometer (Perkin Elmer). The condition was that the wavelength range was 4000 cm^{-1}–500 cm^{-1}, ATR mode. And the molecular structure of M-SMPI and E-SMPI were also tested by ^1H NMR (ADVANCE III 400 MHZ 010601, Bruker), among them, the solvent was deuterated chloroform ($CDCl_3$), and the internal standard was tetramethylsilane (TMS). Dynamic mechanical performance of M-SMPI, E-SMPI and M-SMPI/CF were characterized by DMA Q800 (TA Corporation of American). Test conditions were that stretch mode, N_2 atmosphere, the flow rate of 10.00 mL/min, the temperature rise/fall rate of 5 ℃/min, the temperature range of 25 ℃–560 ℃, 0.2% amplitude, and 1 Hz frequency. The thermal stability of M-SMPI and E-SMPI were tested by TGA/DSC1 synchronous thermal analyzer, produced by METTLER-TOLEDO Corporation, Switzerland. Test conditions were in N_2 atmosphere, the heating rate was 10 ℃/min, the temperature range was 25 ℃–800 ℃, and the weight was 5–10 mg. The tensile properties were tested by Zwick tensile testing machine. The size of M-SMPI and E-SMPI were prepared according to GB/T528-2009 and M-SMPI/CF composites were conducted under the ASTM-D3039 standard. The tensile speed was 5 mm/min, and five specimens of each materials were tested. The interface morphology of M-SMPI/CF composites were observed by the JEM-1200 scanning electron microscope (SEM, JEOL Corporation of Japan). Thermal-actuated shape memory performance was as follows: The sample was heated to $T_g + 30$ ℃ for 5 min, then, it was bent to 180° and dropped the temperature to 25 ℃ under external force for 5 min. At last, the sample was put in $T_g + 30$ ℃ thermal field to achieve the shape

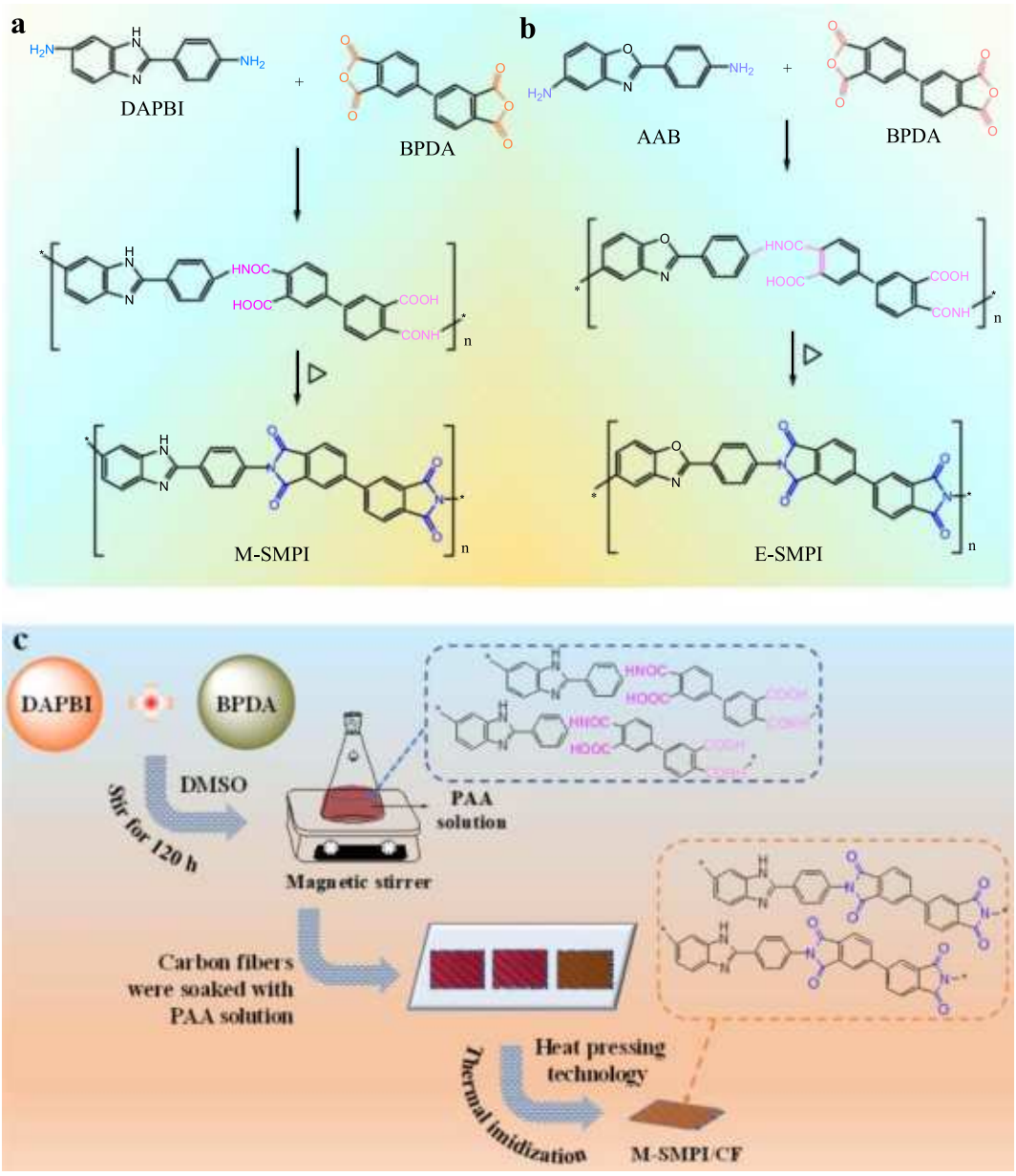

Fig. 1. (a) The synthesis route of imidazole-based shape memory polyimide (M-SMPI), (b) the synthesis route of oxazole-based shape memory polyimide (E-SMPI), (c) the preparation process of the imidazole-based shape memory polyimide/carbon fiber twill fabric composite (M-SMPI/CF). (For interpretation of the references to colour in this figure legend, the reader is referred to the web version of this article.)

recovery. The quantitative shape memory performances of M-SMPI, E-SMPI films and M-SMPI/CF composites were tested by DMA (stretch mode). The test steps were as follows: First, the samples were heated to T_g + 30 ℃, at this time, a certain stress was applied to stretch the samples from strain ε_0 to $\varepsilon_0 + \Delta L$. Then, the samples were reduced to 250 °C, at this time, the loaded stress was removed, and the strain was $\varepsilon_0 + \Delta L$'. Finally, the samples were heated to $T_g + 30$ °C again to obtain the recovery strain ε_{rec}. The heating/cooling rate was 10 ℃/min.

The equation of the shape fixation ratio (R_f) and shape recovery ratio (R_r) were as follows:

$$R_f = \frac{\varepsilon_0 + \Delta L'}{\varepsilon_0 + \Delta L} \times 100\% \cdots\cdots \quad (1)$$

$$R_r = \frac{\varepsilon_{rec}}{\varepsilon_0 + \Delta L'} \times 100\% \cdots\cdots \quad (2)$$

where $\varepsilon_0 + \Delta L$ represented the highest strain value upon external stress, $\varepsilon_0 + \Delta L$' represented the fixed strain value after removing the external stress, and ε_{rec} represented the recovered strain value.

3. Results and discussion

3.1. Molecular structure of the SMPI

On the infrared spectrum of the M-SMPI (Fig. 2a), 3059 cm^{-1} was the aromatic ring's Ar-H stretching vibration peak, and 3346 cm^{-1} was the amine group's N—H stretching vibration peak. In addition, 1774 cm^{-1}, 1706 cm^{-1}, 1351 cm^{-1}, and 722 cm^{-1} were all characteristic absorption peaks of the polyimide. Among them, 1774 cm^{-1} was the stretching vibration peak of the two carbonyl groups on the five-membered imine ring, which was also called imide I band; 1706 cm^{-1} was the corresponding asymmetric stretching vibration peak (imide II band); 1351 cm^{-1} was the —C—N— stretching vibration peak (imide III band); and 722 cm^{-1} was the imine ring's deformation vibration peak (imide IV

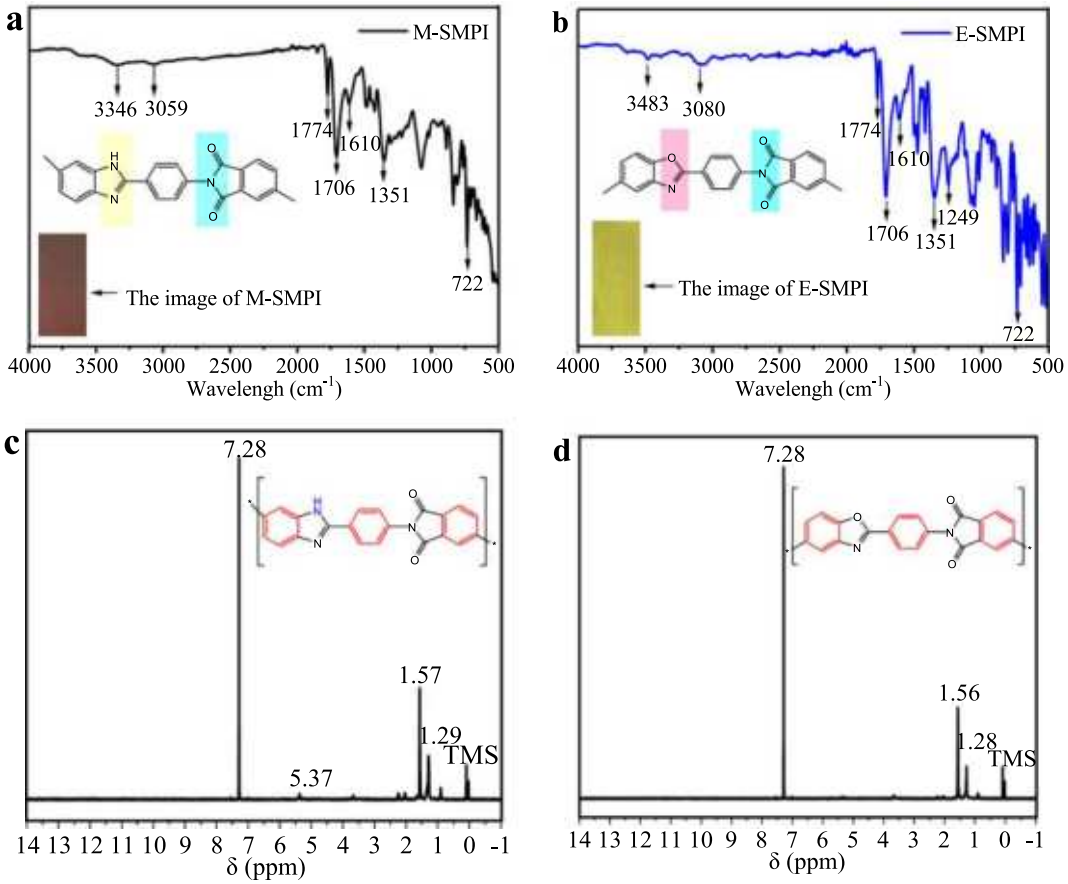

Fig. 2. (a) The FTIR spectrum of M-SMPI, (b) the FTIR spectrum of E-SMPI, (c) the ^{1}H NMR of M-SMPI, (d) the ^{1}H NMR of E-SMPI. (For interpretation of the references to colour in this figure legend, the reader is referred to the web version of this article.)

band), that is, the variable angle vibration of the —C═O. Also, 1610 cm^{-1} was the imidazole ring's C═N characteristic absorption peak. Thus, it showed that imidazole-based shape memory polyimide (M-SMPI) was prepared successfully. On the infrared spectrum of the E-SMPI (Fig. 2b), 3483 cm^{-1} was the amine group's N—H stretching vibration peak, and 3080 cm^{-1} was the aromatic ring's Ar-H stretching vibration peak. Additionally, 1774 cm^{-1}, 1706 cm^{-1}, 1351 cm^{-1}, and 722 cm^{-1} were also characteristic absorption peaks of the polyimide. 1610 cm^{-1} was the oxazole ring's C═N absorption peak, and 1249 cm^{-1} was the —C—O— stretching vibration without hydrogen on the oxazole ring. Hence, it illustrated that oxazole shape memory polyimide (E-SMPI) was synthesized successfully.

Fig. 2c exhibited the ^{1}H NMR spectrum of the M-SMPI, where the chemical shift at $\delta = 7.28$ ppm was the characteristic peak of hydrogen on the benzene ring, that at $\delta = 5.37$ ppm was the characteristic peak of hydrogen on the imidazole ring, and that at $\delta = 1.29$–1.57 ppm was hydrogen's characteristic peak on the —$(CH_3)_2$ in the residual solvent DMSO. Fig. 2d showed the ^{1}H NMR spectrum of the E-SMPI, where the chemical shift at $\delta = 7.28$ ppm was hydrogen's characteristic peak on the benzene ring, and that at $\delta = 1.28$–1.56 ppm was the hydrogen's characteristic peak on the -$(CH_3)_2$ in the residual solvent DMSO. The M-SMPI and E-SMPI both have benzene rings, and the molecular structures are analogous, so, they have similar benzene ring peak. In addition, the adjacent molecular structures all tend to form large π bonds, which have similar effect on the benzene ring peak position, so the chemical shift of the hydrogen on these benzene rings shows in the same position ($\delta =$ 7.28 ppm). The characteristic absorption peak of carboxylic acid —COOH was not displayed in the two NMR spectra, confirming that the polyamic acid was completely thermally imidized to form polyimide.

3.2. Thermodynamic properties of the SMPI

Fig. 3a was the DMA curves of the storage modulus E' of the SMPI films, and Fig. 3b showed the loss factor curves of the SMPI films. The temperature at the highest point of the loss factor curve represented the glass transition temperature (T_g) of the SMPI, which was also the shape memory transition temperature (T_{trans}). From Fig. 3a and Table 1, it illustrated that the storage modulus of the films was continuously reduced during the temperature from 25 °C to 450 °C. The E-SMPI had a wide step in the range of 300 °C–350 °C, which was the range of the glass transition temperature. The storage modulus was rapidly reduced by two orders of magnitude, indicating that the storage modulus changed significantly after glass transition temperature, which was good for the E-SMPI to fix the temporary shape. Similarly, the storage modulus of the M-SMPI also continuously decreased in the range of 350 °C–450 °C, and the glass transition region also appeared in this range. On the Fig. 3b, the E-SMPI had a sharp peak in the range of 300 °C–350 °C, and the position at 334 °C was the highest, therefore, the T_g or the T_{trans} of the E-SMPI was 334 °C. Similarly, the M-SMPI had a sharp peak in the range of 350 °C–450 °C, and the position was the highest at 416 °C, so, the T_g or the T_{trans} of the M-SMPI was 416 °C. It can be seen from the DMA test that the storage modulus and loss factor curves of M-SMPI and E-SMPI were different, which was mainly related to their molecular structure. M-SMPI was synthesized by DAPBI and BPDA monomers containing imidazole rings, while E-SMPI was synthesized by AAB and BPDA monomers containing oxazole rings on the molecular chain segment. The imidazole ring had —N—H polar group, while oxazole ring contained —O— ether bond group, and the difference was that the flexibility of ether bond group was higher than that of —N—H group. So, the flexibility of M-SMPI containing imidazole ring was lower than that of E-

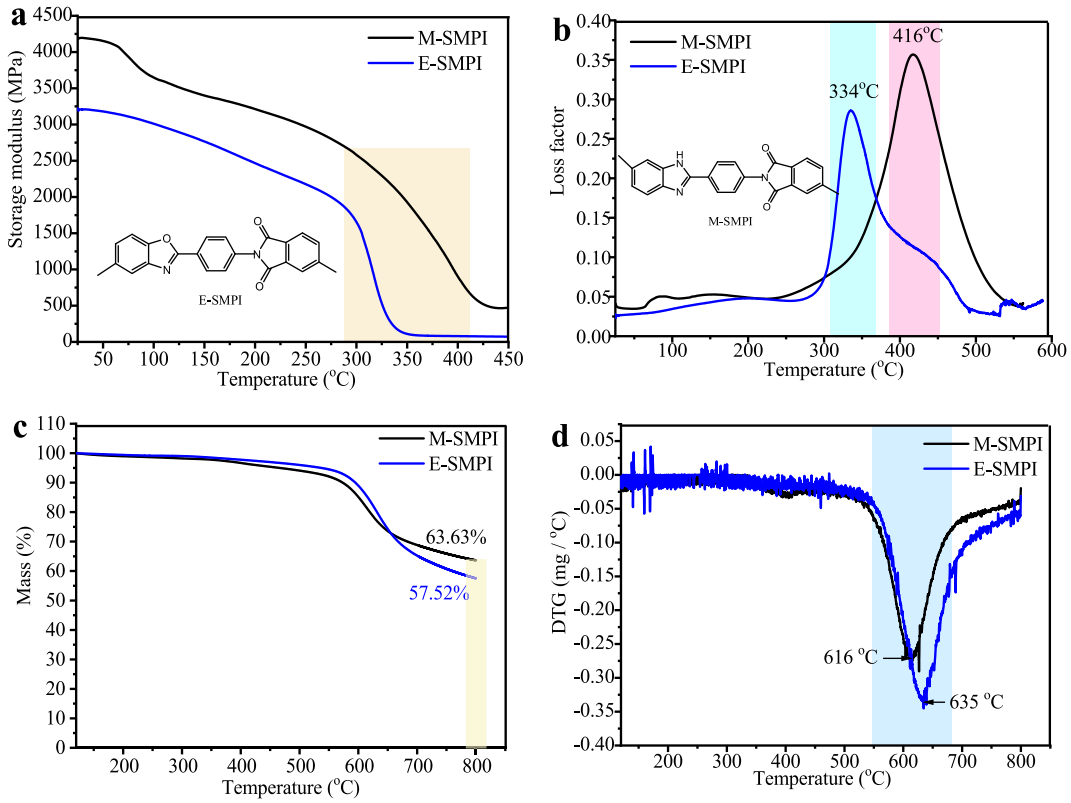

Fig. 3. (a) The storage modulus (E') curves of the M-SMPI and E-SMPI, (b) the loss factor curves of the M-SMPI and E-SMPI, (c) the TG curves of the M-SMPI and E-SMPI, (d) the DTG curves of the M-SMPI and E-SMPI. (For interpretation of the references to colour in this figure legend, the reader is referred to the web version of this article.)

Table 1
Thermomechanical properties of the M-SMPI and E-SMPI films.

	E′ (25℃)/MPa	E′ (200℃)/MPa	E′ (400℃)/MPa	E′ (450℃)/MPa	T_g (℃)
M-SMPI	4183	3213	900	474	416
E-SMPI	3224	2466	80	73	334

SMPI containing oxazole ring. By contrast, the rigidity of the M-SMPI molecular chain segment was greater than that of the E-SMPI, and it was not easy to slip the molecular chain segment during the heating process. As a consequence, the storage modulus and the loss factor peak position of M-SMPI was higher than that of E-SMPI.

TGA test was used to illustrated the thermal stability of the SMPI. Fig. 3c and Fig. 3d showed the TG curves and DTG curves of the SMPI films, respectively. The TG curves of the SMPI were almost flat below 500 ℃, which illustrated that the thermal weight loss was very small, and there was almost no decomposition, only a small amount of water or micro-molecule was volatilized. In the range of 500 ℃–700 ℃, the SMPI underwent rapid decomposition, when the temperature reached 800 ℃, both of them still had more than 50% residual content. It can be seen from the DTG curves that the peak positions of the M-SMPI and E-SMPI were at 616 °C and 635 °C, respectively, so their maximum decomposition rates temperature ($T_{dec,\ max}$) were 616 °C and 635 °C, respectively. Table 2 showed the thermal stability data of the M-SMPI and E-SMPI. It can be seen from the table that the initial decomposition temperature of the M-SMPI, that is, the 5% decomposition temperature ($T_{dec,\ 5\%}$) was 466 ℃, and the residual content at 800 ℃ was 63.63%; the $T_{dec,\ 5\%}$ of the E-SMPI was 537 ℃, and the residual content at 800 ℃ was 57.52%. Because SMPI molecular chains had a large number of aromatic groups, such as benzene ring, aromatic heterocycle and imide, these chemical bonds contained high bond energy and π - π conjugated intermolecular force, which could be broken at high temperature. Hence, the imidazole ring or oxazole ring with higher bonds energy could enhance the overall thermal stability of the SMPI thin films.

Table 2
Thermal stability data of the M-SMPI and E-SMPI films.

	$T_{dec,\ 5\%}$/℃	$T_{dec,\ 10\%}$/℃	$T_{dec,\ max}$/℃	Residual at 800 ℃/%
M-SMPI	466	573	616	63.63
E-SMPI	537	595	635	57.52

3.3. Mechanical properties of the SMPI

Fig. 4 was the stress–strain curves of the M-SMPI and E-SMPI. The maximum tensile strength of the M-SMPI and E-SMPI were 112.9 MPa and 102.5 MPa, respectively, the Young's moduli were 2.0 GPa and 1.9 GPa, respectively, and the elongation at break were 5.3% and 4.6%, successively. In addition, DMA test results showed that the storage moduli of M-SMPI and E-SMPI at room temperature were 4.18 GPa and 3.22 GPa, respectively. Young's modulus and storage modulus were of the same order of magnitude, and both results illustrated that the modulus of M-SMPI was greater than that of E-SMPI, so the tensile test and DMA results were reliable. The mechanical properties of polymers mainly depended on the chemical structure of molecular chain segments, and were also affected by molecular weight and its distribution, cross-linking degree, crystallization, and orientation. The SMPI with

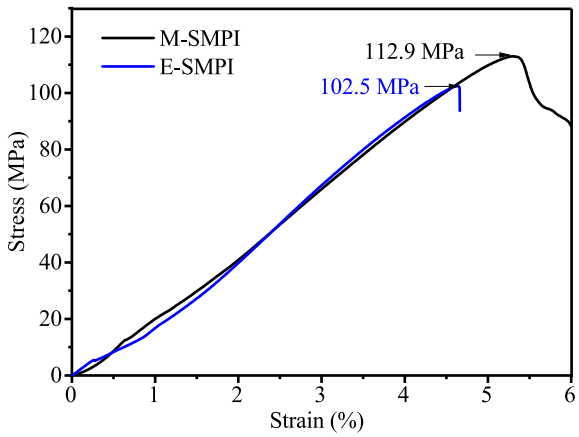

Fig. 4. The tensile mechanical curves of the M-SMPI and E-SMPI. (For interpretation of the references to colour in this figure legend, the reader is referred to the web version of this article.)

aromatic heterocyclic structure had high rigidity, so, the tensile strength was over 100 MPa, and could be used in special occasions such as aerospace, military equipment, and electronics industry. Besides, due to the π-π conjugated system of aromatic heterocycles in the SMPI chain segments cannot rotate internally, the flexibility of the molecular chain segment was reduced but the rigidity was increased. The more the aromatic heterocycles contained, the lower the flexibility of the molecular chain segments had, and the greater the rigidity had. Thus, during the stretching process, the molecular chain segments of the SMPI were difficult to move, resulting in lower elongation at break.

3.4. Shape memory properties of the SMPI

Fig. 5a and b exhibited the shape memory processes of the E-SMPI and M-SMPI, respectively, among them, E-SMPI fully recovered the original shape upon 66 s heating field stimulation, and M-SMPI fully returned to the original shape upon 160 s heating field stimulation. Specifically, E-SMPI was placed in 364 °C environment and it higher than the T_g, then, under the external force, the film was programmed into a "U" shape (i.e. bent 180°) which was held in the room temperature environment. When the external force was removed, the film could fix the temporary shape "U". When heated to 364 °C again, the film could completely recover the original shape after 66 s. Similarly, M-SMPI was placed in 446 °C environment, and then the film was shaped into a "U" shape by external force, and the "U" temporary shape was fixed in a room temperature environment without external force. Heating to 446 ℃ again, the film can return to the original shape after 160 s. Thus, the prepared M-SMPI and E-SMPI both had good thermal-actuated shape memory properties. From the microscopic molecular point of view, the reason why the M-SMPI has shape memory effect is that their molecular chains contain asymmetric imidazole groups, which holds a certain degree of flexibility and rigidity. During the shape recovery process, it can recover from the temporary status to the original status while maintaining high stiffness. Thus, the M-SMPI can be used as smart materials in flexible electronics device, aerospace engineering and deployable structures. Similarly, the E-SMPI molecular chains contain asymmetric oxazole groups, which also has a certain degree of flexibility and acts as a reversible phase to hold the temporary status and returns to the original status upon external reheating stimulation.

Fig. 5c and d were the thermomechanical cycle curves by DMA test, i.e. shape memory process curves of the M-SMPI and E-SMPI, respectively. The figures confirmed that both M-SMPI and E-SMPI had good shape memory effects. Specifically, in Fig. 5c, the shape fixation ratio of the M-SMPI was 84.5%. (The value was calculated by Eq. (1)). And the shape recovery ratio of the M-SMPI was 96.0% (The value was calculated by Eq. (2)). Similarly, in Fig. 5d, the shape fixation ratio and shape recovery ratio of the E-SMPI were 97.4% and 70.9%, respectively. Due to the different rigidity of molecular chain segments, their shape memory capabilities were also different. The molecular chain rigidity of M-SMPI was larger than that of E-SMPI, so the shape fixation ratio of M-SMI was lower than that of E-SMPI, while the shape recovery ratio was higher than that of E-SMPI. The prepared SMPI has shape memory properties, and the mechanism is that the molecular chain segments of the polyimide are physically cross-linked to form a stationary phase and a reversible phase. The stationary phase is composed of π-π interactions between aromatic rings and molecular chain entanglement, and the asymmetric imidazole or oxazole rings act as reversible phases. As shown in Fig. 5e, when the temperature rises over T_g, the microscopic Brownian motion of the reversible phase molecular chains are accelerated, while the stationary phase is still in a solidified status. At this time, the polyimide is deformed by external force, and it can be programmed to a new shape $\varepsilon_0 + \Delta L$. Then, the external force is held until the temperature is lower than the T_g, at this time, the reversible phase molecular chain's motion is "frozen", and the new shape is fixed, that is, namely the temporary shape $\varepsilon_0 + \Delta L$'. After that, the temperature rises over T_g again, the stationary phase remains solidified, while the reversible phase softens and the molecular chain segments "unfreeze". Under the action of the internal recovery stress of the stationary phase, the reversible phase gradually reaches the thermodynamic equilibrium status, macroscopically, the polyimide restores to the original shape ε_{rec}. Due to the huge number of aromatic ring structures, there are strong π-π interactions in the SMPI molecular chains, which is conducive to the shape recovery property. In addition, the SMPI we prepared is thermoplastic material, so, during the shape memory process, a part of molecular chains segments can slip, which have permanent deformations.

3.5. Physical properties of the M-SMPI/CF composites

The above experimental tests illustrated that the M-SMPI had the best comprehensive performance, therefore, the M-SMPI was used as the matrix resin to prepare carbon fiber fabric composites, named M-SMPI/CF composites. Their physical properties, mechanical loading properties, and shape memory properties were characterized by SEM, DMA, and tensile testing machine. Fig. 6a showed the storage modulus curves of the M-SMPI/CF composites, and Fig. 6b showed the loss factor curves. It can be seen from the Fig. 6a that the storage modulus of the M-SMPI/1CF, M-SMPI/2CF, M-SMPI/3CF, and M-SMPI/4CF composites at room temperature were 3.4 GPa, 4.4 GPa, 5.0 GPa, and 7.0 GPa, respectively. In the Fig. 6b, the loss factor peak of the M-SMPI/CF composites were in the range of 350 °C–450 °C, and the highest peak of the M-SMPI/1CF, M-SMPI/2CF, M-SMPI/3CF, and M-SMPI/4CF appeared at 394 °C, 393 °C, 399 °C, and 397 °C, respectively, therefore, the T_g or T_{trans} of the shape memory composites were 394 °C, 393 °C, 399 °C, and 397 °C, respectively. Compared with the pure M-SMPI film, the glass transition temperature decreased by 17 °C–23 °C. This was because the carbon fiber fabrics destroyed the regularity of the polyimide molecular chain segment structures and increased the randomness of the molecular chain segments.

The tensile strength of the M-SMPI/1CF, M-SMPI/2CF, M-SMPI/3CF, and M-SMPI/4CF were shown in Fig. 6c, which were 74.1 MPa, 96.7 MPa, 106.6 MPa, and 122.1 MPa, successively. In addition, the Young's modulus of the M-SMPI/1CF, M-SMPI/2CF, M-SMPI/3CF, and M-SMPI/4CF in the Fig. 6d were 3.0 GPa, 3.1 GPa, 3.5 GPa and 3.6 GPa, successively, while the Young's modulus of the pure M-SMPI was 2.0 GPa. So, the carbon fiber fabrics had a reinforcing effect on the M-SMPI/CF composites. In addition, the cross-sectional morphology and interface morphology of the M-SMPI/CF composites were observed by SEM (Fig. 6e). It can be clearly seen that the surface of the carbon fiber fabrics was rough and uneven with resin fragments, and the exposed resin matrix was uneven. These phenomena indicated that the carbon fiber fabrics and the resin matrix did not delaminate at the interface, and the

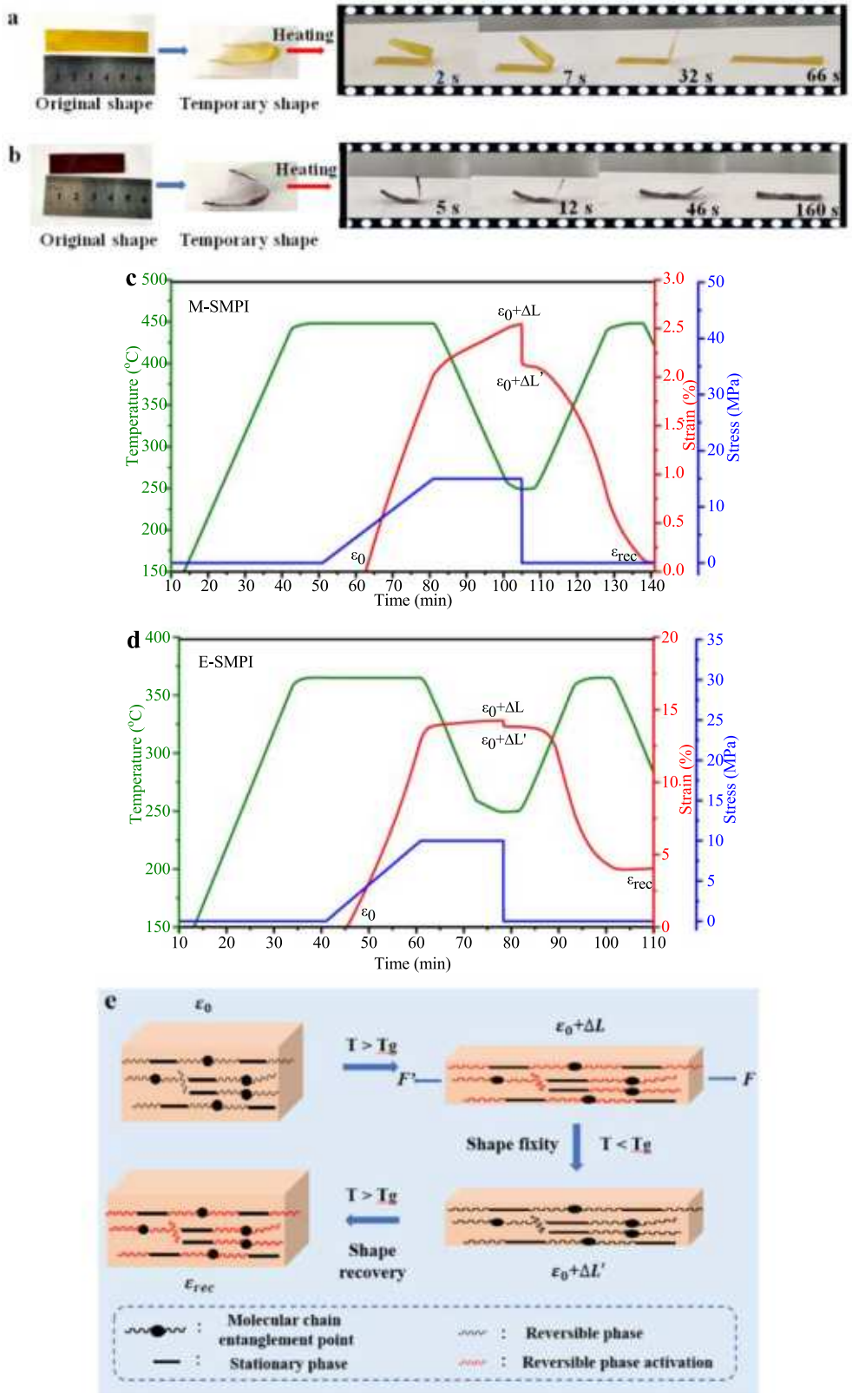

Fig. 5. (a) The images of shape memory process of the E-SMPI, (b) the images of shape memory process of the M-SMPI, (c) the shape memory process curves of the M-SMPI, (d) the shape memory process curves of the E-SMPI, (e) the shape memory mechanism of the SMPI. (For interpretation of the references to colour in this figure legend, the reader is referred to the web version of this article.)

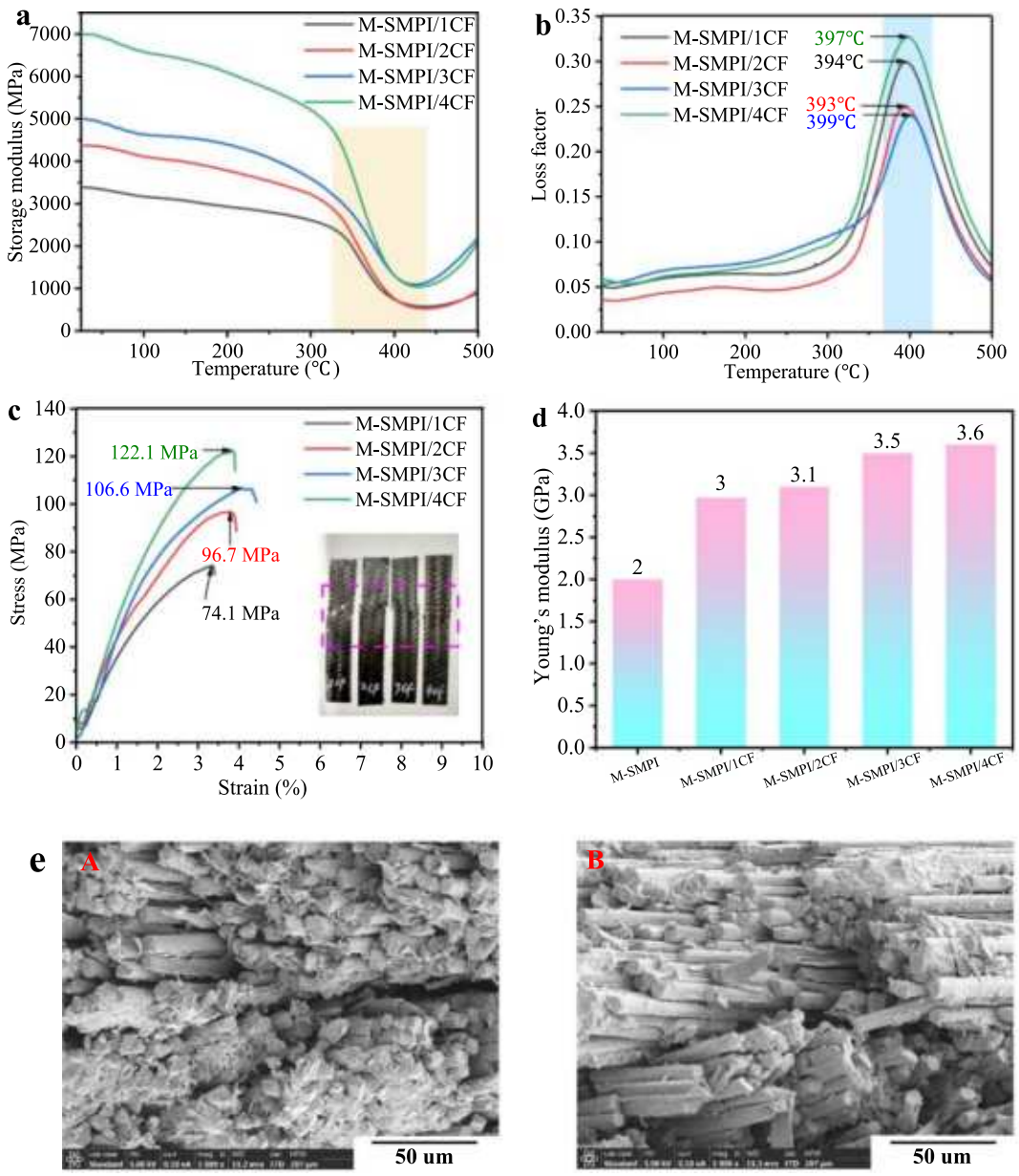

Fig. 6. (a) The storage modulus curves of the shape memory M-SMPI/CF composites, (b) the loss factor curves of the M-SMPI/CF composites, (c) the stress–strain curves of M-SMPI/CF composites, and photos of the stretched M-SMPI/CF composites, from left to right was M-SMPI/1CF, M-SMPI/2CF, M-SMPI/3CF, and M-SMPI/4CF, respectively, (d) the Young's modulus of M-SMPI and M-SMPI/CF composites, (e) SEM images of the shape memory M-SMPI/CF composites, A and B were M-SMPI/1CF and M-SMPI/3CF, respectively. (For interpretation of the references to colour in this figure legend, the reader is referred to the web version of this article.)

two phases were combined well. The reason is that the carbon fiber fabrics are immersed in the polyamic acid (PAA) solution with carboxyl groups, which can improve the interfacial bonding ability between the resin and fibers, and after hot pressing and secondary thermal imidization process, the PAA has imidization to form polyimide. The polyimide contains benzene rings, aromatic heterocyclic rings and imide rings, a large number of hydrogen bonds and intermolecular forces, hence, the interface between the carbon fibers and the M-SMPI matrix is well bonded.

3.6. Shape memory properties of the M-SMPI/CF composites

Shape memory performance of the M-SMPI/CF composite was qualitatively verified by bending and bending recovery test. Fig. 7a showed the shape recovery process of the M-SMPI/3CF composite. After being bent at 180° and reheated for 80 s, the composite can return to its original shape. In order to demonstrate the recovery stress of the M-SMPI/3CF composite in a more practical way, 0.82 g M-SMPI/3CF composite strip was processed into a primitive actuator, and its performance was shown in Fig. 7b. The 6.50 g square steel ingot was placed on the actuator, and the actuator could overturn the square steel ingot upon heating for 236 s. (The process of primitive actuator overturning a square steel ingot was shown in Supporting Information, video 1.) Therefore, the smart composite could overturn objects nearly ten times heavier than its own weight and can be used as a load-bearing member and has important applications in the field of high temperature active deformation. In addition, we also demonstrated the automatic unfolding of the corrugated shape of the SMPI/3CF composite, as shown in Fig. 7c. After being bent to the corrugated shape and heated for 60 s, the composite can unfold and recover the original status. (The process of corrugated shape recovery was shown in Supporting Information, video 2.) We know that the research foundation of deformable aircraft is

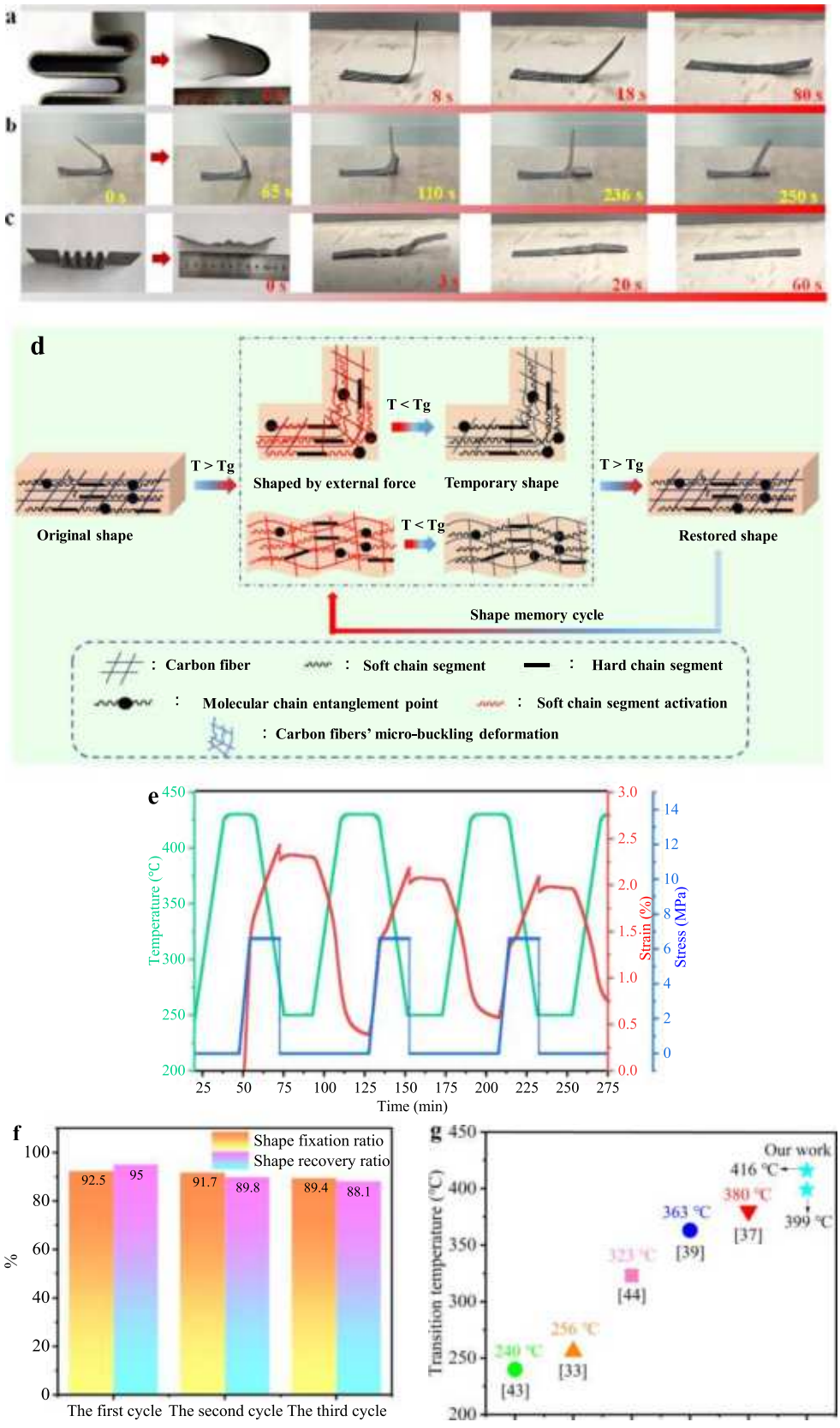

Fig. 7. (a) Photos of the "U" shape recovery processes of the M-SMPI/3CF composite, (b) a primitive actuator made of 0.82 g M-SMPI/3CF composite overturning 6.50 g square steel ingot, (c) photos of the corrugated shape recovery processes of the M-SMPI/3CF composite, (d) shape memory mechanism of the M-SMPI/CF composite, (e) shape memory cycle curves of the M-SMPI/3CF composite, (f) shape memory properties of the M-SMPI/3CF with three cycles, (g) comparison of transition temperature with other literatures. (For interpretation of the references to colour in this figure legend, the reader is referred to the web version of this article.)

various active morphing wings and active aeroelastic wings, and the morphing wings based on intelligent structure has become the forefront of the aviation science and technology at home and abroad. Thus, the shape memory SMPI/CF composite can be used as the skin material of the morphing wings and has broad application prospects.

The shape memory mechanism of SMPI/CF composites is shown in Fig. 7d. The shape memory effect realization of the shape memory carbon fiber composites mainly comes from the staged structural

changes of resins and fibers with temperature changing, including the transition of resin matrices between glass status and high elastic status, and the transition of fibers between flat status and buckling status. The shape memory cycle process can be divided into the following stages: (I) Folded stage: the temperature of the composite is higher than its T_g, and the resin matrix enters a high elastic status, at this time, the shear modulus is low and the bending resistance is poor. When the bending strain of the composite gradually increases to the critical strain, the fibers cannot be effectively bound due to the lower shear modulus of the matrix. As a result, the fibers are forced to buckling in the compression zone, and the composite undergoes a large bending deformation. (II) Fixed stage: maintaining the external force, keeping the bending deformation, and reducing the temperature below the glass transition temperature can constrain the molecular chain segments in the matrix. Macroscopically, the resin matrix hardens, and the shear modulus rises, at this time, the matrix can effectively restrain the fibers. When the external force is removed, the micro-buckling deformation of the fibers and the deformation of the matrix itself are fixed. (III) Unfolded stage: when the temperature rises over the glass transition temperature again, the shear modulus of the matrix decreases again, and the elastic potential energy stored in the buckling fibers is released; at the same time, the strain energy stored in the matrix is also released, macroscopically, the composite unfolds and returns to its original status.

DMA was used to quantitatively exhibit the shape memory performance of the M-SMPI/CF composites. Fig. 7e was the thermomechanical cycle curves of the M-SMPI/3CF, and Fig. 7f was the shape memory properties of the M-SMPI/3CF with three cycles. Among them, the shape fixation ratio of the M-SMPI/3CF composite was 92.5% and the shape recovery ratio was 95.0% in the first shape memory cycle. And the shape fixation ratio was 91.7% and the shape recovery ratio was 89.8% in the second cycle. And the shape fixation ratio was 89.4% and the shape recovery ratio was 88.1% in the third cycle. As the thermomechanical cycles gradually increase, the shape memory properties of the SMPI/CF composites gradually decrease. This is because the carbon fiber fabrics have elastic recovery property, which leads to the shape fixation ratio decrease during the shape fixation stage. Additionally, the SMPI/CF composite has structural variance in the thermomechanical cycle processes, such as fiber fracture, resin matrix molecular chain fracture, and the decrease of the interfacial adhesion, therefore reducing the shape memory properties. The T_{trans} of the SMPI was compared with that reported in other literatures [33,37,39,43,44], as shown in Fig. 7g. The results showed that the T_{trans} of common SMPIs were generally below 380 ℃, however, our work can reach over 400 ℃.

4. Conclusions

In this paper, we synthesize two semi-trapezoidal aromatic heterocyclic shape memory polyimides, including imidazole-based shape memory polyimide (M-SMPI) and oxazole-based shape memory polyimide (E-SMPI), which is illustrated by FTIR and ^{1}H NMR. DMA test shows that the glass transition temperature of the M-SMPI and E-SMPI are 416 ℃ and 334 ℃, respectively. TGA test shows that both of them have good thermal stabilities. The thermomechanical cycle test illustrates that the shape fixation ratio of the M-SMPI and E-SMPI are 84% and 99%, respectively, and the shape recovery ratio are 96% and 71%, respectively, thus, chain stiffness has a significant effect on the shape memory properties of SMPI. Additionally, we prepare shape memory composites M-SMPI/3CF, of which the shape fixation ratio and recovery ratio are 92.5% and 95.0% in the first cycle, respectively, and the Young's modulus is 3.5 GPa. Therefore, the SMPIs and composites with tunable chain stiffness and ultrahigh transition temperature range have huge potential application in flexible electronics and aerospace engineering.

CRediT authorship contribution statement

Xiaofei Wang: Investigation, Methodology, Data curation, Visualization, Writing – original draft, Writing – review & editing. **Yang He:** Investigation, Methodology, Validation, Resources, Project administration, Writing – review & editing. **Jinsong Leng:** Conceptualization, Supervision, Project administration, Funding acquisition, Writing – review & editing.

Declaration of Competing Interest

The authors declare that they have no known competing financial interests or personal relationships that could have appeared to influence the work reported in this paper.

Data availability

Data will be made available on request.

Acknowledgements

This work was supported by the Heilongjiang Touyan Innovation Team Program.

Appendix A. Supplementary material

Supplementary data to this article can be found online at https://doi.org/10.1016/j.compositesa.2022.107237.

References

[1] Kong D, Li J, Guo A, Xiao X. High temperature electromagnetic shielding shape memory polymer composite. Chem Eng J 2021;408:127365.
[2] Liang R, Yu H, Wang Li, Amin BU, Wang N, Fu J, et al. Triple and two-way reversible shape memory polymer networks with body temperature and water responsiveness. Chem Mater 2021;33(4):1190–200.
[3] Jeong HY, Woo BH, Kin N, Jun YC. Multicolor 4D printing of shape-memory polymers for light-induced selective heating and remote actuation. Sci Rep 2020;10(1):6258.
[4] Gong X, Tan K, Deng Q, Shen SP. A thermal shape memory effect in magnetoactive elastomers. ACS Appl Mater Interf 2020;12(14):16930–6.
[5] Liu T, Liu L, Yu M, Li Q, Zeng C, Lan X, et al. Integrative hinge based on shape memory polymer composites: Material, design, properties and application. Compos Struct 2018;206:164–76.
[6] Wan X, Zhang FH, Liu YJ, Leng JS. CNT-based electro-responsive shape memory functionalized 3D printed nanocomposites for liquid sensors. Carbon 2019;155:77–87.
[7] Kashirina A, Yao YT, Liu YJ, Leng JS. Biopolymers as bone substitutes: a review. Biomater Sci 2019;7(10):3961–83.
[8] Chen H, Zhang F, Sun Ya, Sun B, Gu B, Leng J, et al. Electrothermal shape memory behavior and recovery force of four-dimensional printed continuous carbon fiber/polylactic acid composite. Smart Mater Struct 2021;30(2):025040.
[9] Xin X, Liu L, Liu Y, Leng J. Origami-inspired self-deployment 4D printed honeycomb sandwich structure with large shape transformation. Smart Mater Struct 2020;29(6):065015.
[10] Zhao H, Lan X, Liu L, Liu Y, Leng J. Design and analysis of shockless smart releasing device based on shape memory polymer composites. Compos Struct 2019;223:110958.
[11] Xiao R, Zhang C, Gou XF, Huang WM. Tunable shape-memory behaviors in amorphous polymers through bound solvent. Mater Lett 2017;209:131–3.
[12] Hubbard AM, Davis DS, Dickey MD, Genzer J. Shape memory polymers for self-folding via compression of thermoplastic sheets. J Appl Polym Sci 2018;135(47):46889.
[13] Liu C, Qin H, Mather BPT. Review of process in shape memory polymer. J Mater Chem 2007;17(16):1543–58.
[14] Kong D, Li J, Guo A, Yu J, Xiao X. Smart polyimide with recovery stress at the level of high temperature shape memory alloys. Smart Mater Struct 2021;30(3):035027.
[15] Holman H, Kavarana MN, Rajab TK. Smart materials in cardiovascular implants: shape memory alloys and shape memory polymers. Artif Organs 2020;45(5):454–63.
[16] Basit A, Lhostis G, Durand B. Investigation of the shape memory and actuation properties of different asymmetric smart polymer composites. Adv Compos Mater 2020;30(5):462–77.
[17] Kim CL, Lee JJ, Oh YJ, Kim DE. Smart wearable heaters with high durability, flexibility, water-repellent and shape memory characteristics. Compos Sci Technol 2017;152:173–80.

[18] Shikinaka K, Funatsu Y, Kubota Y, Tominaga Y, Nakamura M, Navarro RR, et al. Tuneable shape-memory properties of composites based on nanoparticulated plant biomass, lignin, and poly(ethylene carbonate). Soft Matter 2018;14(45):9227–31.
[19] Chen S, Cao Y, Sarparast M, Yuan H, Dong L, Tan X, et al. Soft crawling robots: design, actuation, and locomotion. Adv Mater Technol 2020;5(2):1900837.
[20] Kuzyk MG, Dawson NJ. Photomechanical materials and applications: a tutorial. Adv Opt Photon 2020;12(4):847–1011.
[21] Shukla G, Pandey RP, Shahi VK. Temperature resistant phosphorylated graphene oxide-sulphonated polyimide composite cation exchange membrane for water desalination with improved performance. J Membr Sci 2016;520:972–82.
[22] Ma P, Dai C, Wang H, Li Z, Liu H, Li W, et al. A review on high temperature resistant polyimide films: Heterocyclic structures and nanocomposites. Compos Commun 2019;16:84–93.
[23] Lu TD, Zhao LL, Yong WF, Wang Q, Duan L, Sun SP. Highly solvent-durable thin-film molecular sieve membranes with insoluble polyimide nanofibrous substrate. Chem Eng J 2021;409:128206.
[24] Haruki M, Tanaka K, Tada J, Onishi H, Tada Y. Effective thermal conductivity for nanocarbon/polyimide and carbon nanofiber/hexagonal boron nitride/polyimide composites. Polym Compos 2019;40(8):3032–9.
[25] Choi JY, Lee J, Jeon J, Im J, Jang J, Jin SW, et al. High-performance non-volatile resistive switching memory based on a polyimide/graphene oxide nanocomposite. Polym Chem 2020;11(48):7685–95.
[26] Svetlichnyi VM, Kudryavtsev VV. Polyimides and the problems of designing advanced structural composite materials. Polym Sci Ser B 2003;45(5–6):140–85.
[27] Wen Y, Meng XS, Liu JF, Yan JL, Wang Z. Surface modification of high-performance polyimide fibers by oxygen plasma treatment. High Perform Polym 2017;29(9):1083–9.
[28] Liu N, Liu Y, Zhao Y, Liu Y, Lan Q, Qin J, et al. CNT-Intertwined polymer electrode toward the practical application of wearable devices. ACS Appl Mater Interf 2019;11(50):46726–34.
[29] Ogbonna VE, Popoola API, Popoola OM, Adeosun SO. A review on polyimide reinforced nanocomposites for mechanical, thermal, and electrical insulation application: challenges and recommendations for future improvement. Polym Bull 2020;79(1):663–95.
[30] Rafidah RSR, Rashmi W, Khalid M, Wong WY, Priyanka J. Recent progress in the development of aromatic polymer-based proton exchange membranes for fuel cell applications. Polymers 2020;12(5):1061.
[31] Yao J, Ma S, Zhang J, Wang Y, Wang C, Zhou H, et al. Multiple shape memory effects of polyimide nanocomposites based on octa(aminophenyl) silsequioxanes. Exp Polym Lett 2021;15(5):433–44.
[32] Kong D, Li J, Guo A, Zhang X, Xiao X. Self-healing high temperature shape memory polymer. Eur Polym J 2019;120:109279.
[33] Zhang Z, Kong D, Li X, Ao X, Xiao X. High temperature shape memory polymer with high wear resistance. Smart Mater Struct 2019;28(10):105005.
[34] Yang ZH, Zhang YM, Li S, Zhang XR, Wang TM, Wang QH. Fully closed-loop recyclable thermosetting shape memory polyimide. ACS Sust Chem Eng 2020;8(51):18869–78.
[35] Huang X, Zhang F, Leng J. Metal mesh embedded in colorless shape memory polyimide for flexible transparent electric-heater and actuators. Appl Mater Today 2020;21:100797.
[36] Gao H, Li JR, Xie F, Liu YJ, Leng JS. A novel low colored and transparent shape memory copolyimide and its durability in space thermal cycling environments. Polymer 2018;156:121–7.
[37] Lan ZX, Chen XL, Zhang X, Zhu CY, Yu YL, Wei J. Transparent, high glass-transition temperature, shape memory hybrid polyimides based on polyhedral oligomeric silsesquioxane. Polymers 2019;11(6):1058.
[38] Yu XH, Liang WH, Cao JH, Wu DY. Mixed rigid and flexible component design for high performance polyimide films. Polymers 2017;9(9):451.
[39] Ao XL, Kong DY, Zhang ZY, Xiao XL. Enhancing recovery speed and anti-wear capability of high-temperature shape memory polymer with modified boron nitride nanoparticles. J Mater Sci 2020;55(10):4292–302.
[40] Yang ZH, Chen Y, Wang QH, Wang TM. High performance multiple-shape memory behaviors of poly(benzoxazole-co-imide)s. Polymer 2016;88:19–28.
[41] Yang Z, Song F, Wang Q, Wang T. Shape memory induced structural evolution of high performance copolyimides. J Polym Sci Pol Chem 2016;54(24):3858–67.
[42] Chen YT, Zhang QH. Synthesis, characterization and properties of aromatic copolyimides containing Bi-benzimidazole moiety. J Polym Res 2015;22(5):78.
[43] Xiao X, Kong D, Qiu X, Zhang W, Liu Y, Zhang S, et al. Shape memory polymers with high and low temperature resistant properties. Sci Rep 2015;5(1).
[44] Xiao X, Kong D, Qiu X, Zhang W, Zhang F, Liu L, et al. Shape memory polymers with adjustable high glass transition temperatures. Macromolecules 2015;48(11):3582–9.